

# The relationship between eDNA density distribution and current fields around an artificial reef in the waters of Tateyama Bay, Japan

Nariaki Inoue<sup>1</sup>, Masaaki Sato<sup>1</sup>, Naoki Furuichi<sup>1</sup>, Tomohito Imaizumi<sup>1</sup>, Masayuki Ushio<sup>2,3</sup>

<sup>1</sup> Fisheries Engineering Division, Fisheries Technology Institute, Japan Fisheries Research and Education Agency (FRA), Kamisu, Ibaraki 7620-7, Japan

<sup>2</sup> Hakubi Center, Kyoto University, Kyoto 606-8501, Japan

<sup>3</sup> Center for Ecological Research, Kyoto University, Otsu, Shiga 520-2113, Japan

Corresponding author: Nariaki Inoue ([inoue\\_nariaki87@fra.go.jp](mailto:inoue_nariaki87@fra.go.jp))

Academic editor: Anastasija Zaiko | Received 6 June 2022 | Accepted 28 August 2022 | Published 23 September 2022

## Abstract

Monitoring of artificial reefs (ARs) has been conducted through such methods as visual censuses, surveys using fishing gear, and echo sounder. These methods have disadvantages: visual census is not possible at ARs in deeper waters, fishing gear surveys are invasive to fish individuals, and echo sounders have difficulty in species identification. A new AR monitoring method is required to compensate for these disadvantages. While eDNA has become a valid monitoring tool for marine biodiversities, it is influenced by degradation and transport of the molecules that affect information about the spatio-temporal distribution of fish. An understanding of the relationship between current fields and eDNA distribution, particularly in open waters, is critical when using eDNA as an index for fish aggregation at ARs. We investigated the relationship between eDNA distribution and current fields around an AR for four dominant species (*Engraulis japonicus*, *Parapristipoma trilineatum*, *Scomber* spp and *Trachurus japonicus*) in Tateyama Bay, Japan. The highest density of fish schools is formed directly above or at the upstream side of ARs. If we assume that the center of eDNA originates at these locations at an AR and eDNA is simply transported by currents, a higher density of eDNA would distribute downstream from the AR. However, our results indicate that eDNA distribution is in accord with actual fish distribution, namely eDNA densities are more abundant in the upstream side of ARs. We thus consider that eDNA distribution is more influenced by actual distribution patterns than by the transport processes.

## Key Words

ADCP, artificial reef, current, environmental DNA, fish

## Introduction

Artificial reefs (ARs) are thought to improve fishing by promoting fish aggregation and functioning as both a nursery area and a habitat for juveniles, thereby increasing fisheries stocks in terms of diversity and abundance (Bohnsack and Sutherland 1985). The deployment of ARs has increased since the 1960s, becoming a world-wide practice, especially in the marine ecosystems of Japan, the USA, and Western Europe (Lima et al. 2019). In 1971, the Japanese government started a national project to maintain and develop coastal fisheries, spending at least US\$5.4 billion until recent years to deploy ARs

throughout coastal waters (Sato et al. 2021). Although numerous studies on the effects of ARs on fish aggregation and stock enhancement have been conducted, most of them are not quantitative but qualitative in their assessment (Bohnsack and Sutherland 1985). Few studies have estimated the effect of ARs on gradually increasing fish aggregation and fisheries stocks through quantitative methods (Inoue et al. 2018). Artificial reefs have an average lifetime of 30–50 years until they disintegrate. Continuous long-term monitoring and quantitative assessments of AR effects are needed to improve AR installation plans (installation depth, layout, structure, etc.) and help fishery operations adapt to the effects of aging ARs.

After ARs were installed in Japanese waters, underwater visual censuses, surveys using fishing gear, and echo sounder surveys were conducted to examine fish aggregation and stock enhancement effects of the ARs (Polovina and Sakai 1989; Kakimoto 1993; Kang et al 2011; Inoue et al. 2018). Underwater visual censuses are effective for species identification, fish counts and size estimations; however identification skills *in situ* and/or extended investigation times are required for large areas, and it may not be possible at ARs in deeper waters (Sato et al. 2021). Surveys with bottom trawls and gillnets, which require considerable fishing effort, can obtain information on fish in a way that is similar to underwater visual censuses, but these surveys are invasive to fish individuals as well as the whole ecosystem, depending on the fishing gear used (e.g., the seafloor from trawling). While echo sounders can survey large geographical areas quickly without collecting fish, identifications of fish species are generally not possible. A new method of monitoring ARs that can compensate for the disadvantages of such traditional methods is required.

Researchers have recently begun to use environmental DNA (eDNA) – DNA derived from environmental samples such as water – to investigate the distribution of aquatic organisms, including marine fishes (Minamoto et al. 2017; Yamamoto et al. 2017; Ushio et al. 2018; Komai et al. 2019). The eDNA originates from metabolic waste, damaged tissue, dead individuals, or spawning events for organisms (Barnes and Turner 2016), and the eDNA contains information on taxa and functional genes in a given environment (Taberlet et al. 2018). This method can identify target organisms noninvasively. The eDNA metabarcoding approach, which uses high-throughput sequencing (HTS) technologies and universal primer sets such as MiFish (Miya et al. 2015), has been utilized to reveal fish diversity in a given area (Port et al. 2016; Yamamoto et al. 2016). Port et al. (2016) conducted an eDNA distribution survey to reveal vertebrate fauna in a kelp forest at Monterey Peninsula in California, USA, and a survey conducted in Maizuru Bay, Sea of Japan, Yamamoto et al. (2016) reported a close association between the amount of eDNA distribution and the biomass of the Japanese jack mackerel (*Trachurus japonicus*) surveyed using echo sounder technology. Furthermore, Ushio et al (2018) have developed a method that utilizes internal standard DNAs (i.e. known amounts of short DNA fragments from fish species that have never been observed in a study area) to convert the HTS sequence reads of DNAs to the number of DNA copies in each fish species. Ushio et al (2018) have shown that the actual fish densities of multiple species can be reasonably estimated from DNA copies that are converted using internal standard DNAs. Sato et al. (2021), who were the first to apply the eDNA approach in assessing the AR effect, used Ushio et al (2018)'s method for eDNA density (copy number) estimation to reveal higher densities of fish eDNA at the ARs than in surrounding waters and found that the densities decreased rapidly with distance from the AR and corresponded to actual fish distribution patterns. These findings suggested that eDNA-based fish community monitoring would

provide complementary information about fish community dynamics around ARs to traditional methods.

The distribution pattern of eDNA density in waters reflects not only the spatio-temporal distribution of target fish abundance but is also affected by the degradation and transport of eDNAs (Goldberg et al. 2016). In particular, the process of transport by currents could have a greater influence on the spatial distribution of eDNA densities in open waters, where currents are generally stronger than in semi-enclosed waters. Few studies, however, have assessed an association between current fields and fish eDNA density in the sea (c.f. Murakami et al. 2019). Understanding the relationship between current fields and eDNA density distribution, particularly in open waters, is critical when using eDNA density as an index of fish abundance for assessments of fishery stocks in coastal ecosystems including those around ARs.

It is well known that dense schools of fish are more abundant in the upstream side of ARs (Kakimoto 1967; Okamoto et al. 1979; Lindqvist and Pietrafesa 1989; Holland et al. 2021). Fishing at ARs is very popular in waters off Iki and Tsushima Islands in Nagasaki, Japan (Inoue et al. 2018, 2020), and local fishermen have direct experience with this behavior of fish. They take advantage of this behavior by anchoring the ship at the upstream side of the AR and then aiming fishing gear toward the AR where fish schools are formed by the current. However, Holland et al. (2021) was one of only a few studies that quantitatively assessed the relationship between current fields and fish school formation. This study used statistical model predictions based on multi-beam echosounders (MBES) survey data to evaluate the effect of the occurrence of fish schools on AR waters and found that schools were almost twice as likely to occur upstream than downstream of the ARs.

In this study, we investigate whether fish eDNA density is (i) higher in the upstream than the downstream or (ii) higher in the downstream waters of ARs. In the case of (i), it is likely that eDNA density precisely reflects the actual spatio-temporal distribution of fish abundance. On the other hand, in the case of (ii), eDNA density can be more strongly affected by a transport process caused by the current than actual fish distribution.

In addition to eDNA metabarcoding that was used to survey fish eDNA distribution, an acoustic Doppler current profiler (ADCP), a device that measures water current velocities over a range of depth, was used to investigate the current field around an AR in Tateyama Bay, central Japan. Both datasets enabled us to assess fish eDNA density distributions and their association with the current field around the AR in Tateyama Bay.

This study specifically identified the relationship between eDNA density distribution, current field, and distance from the AR to test whether fish eDNA densities were higher in the upstream than the downstream side of the AR and therefore better reflected actual fish distribution than a transport process. Based on these results, we discuss the effectiveness of eDNA as a monitoring index for fish abundance around ARs.

## Materials and methods

### Study site and water sampling

The field survey was performed in Tateyama Bay, central Japan, in the proximity of the Kuroshio warm current facing the Pacific Ocean (Fig. 1). Many ARs have been implemented in this area. In our study, we focused on the highest steel AR (UT-304, Shinko Kenzai Ltd., Tokyo, Japan) at 34°59'44"N, 139°47'30"E, which is 30 m in height deployed at a depth of 75 m in the waters of Tateyama Bay and has a higher density of fish species than other ARs (Sato et al. 2021). Water sampling for eDNA analysis was undertaken on June 3 (Day 1) and 4 (Day 2), 2019, on board the R/V Taka-maru (Japan Fisheries Research and Education Agency: FRA). Sampling stations were set up at the AR and at three distant points (0.1, 0.2, and 0.4 nautical miles; 0.1 miles  $\approx$  185 m) extending from the AR in four directions (Fig. 1). Sampling was conducted on Days 1 and 2 at a total of 13 stations (due to the lack of survey time by the vessel, excluding the southern three stations on Day 2). Details of the sampling procedure are shown in Suppl. material 1: Table S1.

At each sampling station, 10 L of seawater was collected from a depth of 40 m, which is about the same depth

as the AR except for St. S3, using one cast of two Niskin water samplers (5 L  $\times$  2 samples) (Fig. 1). At St. S3, whose depth is shallower than 40 m, seawater was collected from 20 m depth using the same method with Niskin water samplers. At the AR, we additionally collected 10 L of seawater from the surface using a bucket and 10 L from the bottom (70 m depth) using one cast of two Niskin samplers of the same type. Two 2-L samples were subsampled from the 10-L seawater sample using a measuring bottle, and the remaining 6 L of seawater was used to pre-wash the devices used. Then, in a laboratory on the R/V Taka-maru, following the method described by Miya et al. (2016), two 2-L samples were immediately filtered using a combination of Sterivex filter cartridges (nominal pore size = 0.45  $\mu$ m; SVHV010RS, Merck Millipore, Darmstadt, Germany) through an aspirator. After filtration, 1.5 ml of RNAlater (ThermoFisher Scientific, Waltham, MA, USA) was injected into the cartridge to prevent eDNA degradation. The Niskin water samplers and bucket were bleached before each water collection using a commercial bleach solution, while filtering devices were bleached after each filtration. Two L of MilliQ water were filtered with a filter funnel and measuring cup for each day as a field negative control to test for possible contamination. The filter cartridges were placed in a freezer and stored at below  $-30^{\circ}\text{C}$  immediately after filtration until eDNA extraction.

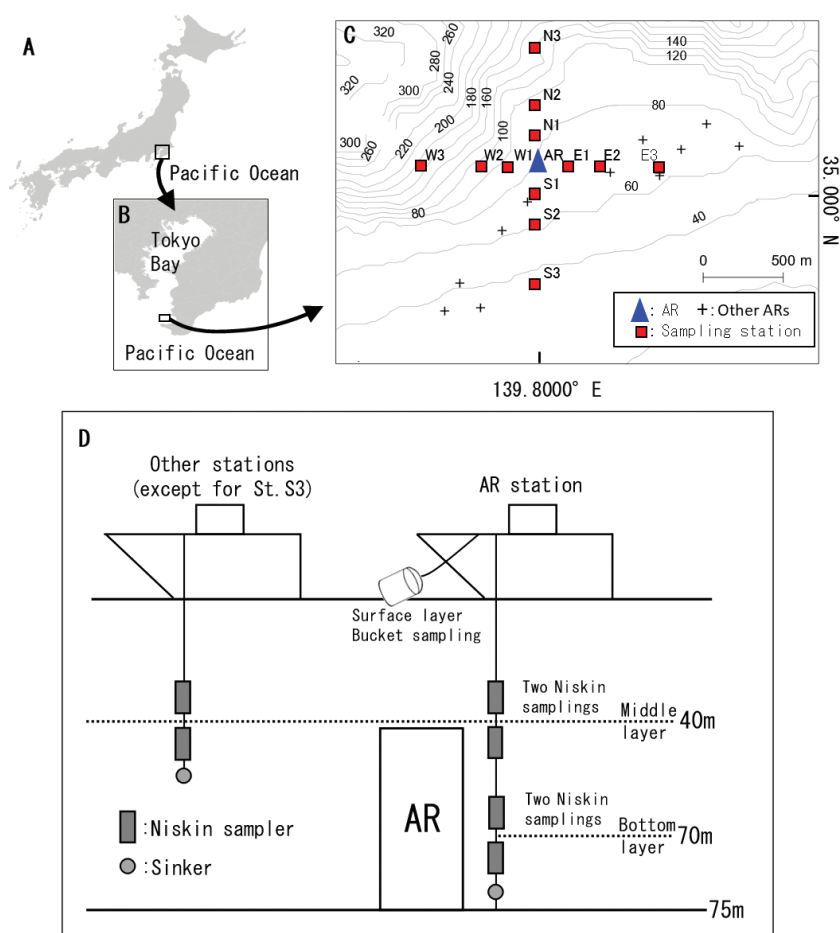


**Figure 1.** Maps showing the wider sampling area encompassing Japan (A), Tokyo Bay (B), and sampling stations (C). Schematic diagram of the water sampling method (D).

## DNA extraction, purification, and PCR

The eDNA was extracted and purified following the method developed by Miya et al. (2016). After removing RNA later from inside the cartridge using a centrifuge, a mixture 60 µl of proteinase-K, 660 µl of phosphate buffered saline, and 600 µl of buffer AL was injected into the cartridge and incubated at 56 °C for 20 min. The eDNA extracts were transferred to a 2-ml tube from the inlet of the filter cartridges by centrifugation. The collected DNA was purified using a DNeasy Blood & Tissue Kit (Qia-gen, Venlo, Netherlands) following the manufacturer's protocol. After purification, DNA was eluted in 100 µl AE buffer and were frozen at -20 °C.

For quantitative MiSeq sequencing, five artificially designed internal standard DNAs (Ushio et al. 2018; Ushio 2019) were used to calculate standard curves to estimate the DNA copy numbers. The copy numbers of the five standard which were artificially designed and synthetic, A to D DNAs were adjusted to 100, 50, 25, 12.5, and 2.5 copies µl<sup>-1</sup>. Sequences of the five standard DNAs are shown in Suppl. material 1: Table S2. Two PCR-level negative controls (i.e. with and without internal standard DNAs) were employed for the MiSeq run to monitor contamination during the experiments.

The first-round PCR (1<sup>st</sup> PCR) was carried out with a 12-µl reaction volume containing 6.0 µl of 2× KAPA HiFi HotStart ReadyMix (KAPA Biosystems, Wilmington, WA, USA), 0.7 µl of each primer (5 µM), 2.6 µl of sterilized distilled H<sub>2</sub>O, 1.0 µl of standard DNA mix, and 1.0 µl of template. The standard DNA mix was included for each sample. The final concentration of each primer was 0.3 µM. A mixture of the following four PCR primers modified from original MiFish primers was used (Miya et al. 2015): MiFish-U-forward (5'-ACA CTC TTT CCC TAC ACG ACG CTC TTC CGA TCT NNN NN G TCG GTA AAA CTC GTG CCA GC) and MiFish-U-reverse (5'-GTG ACT GGA GTT CAG ACG TGT GCT CTT CCG ATC TNN NNN CAT AGT GGG GTA TCT AAT CCC AGT TTG-3'), MiFish-E-forward (5'-ACA CTC TTT CCC TAC ACG ACG CTC TTC CGA TCT NNN NNG TTG GTA AAT CTC GTG CCA GC-3') and MiFish-E-reverse (5'-GTG ACT GGA GTT CAG ACG TGT GCT CTT CCG ATC TNN NNN CAT AGT GGG GTA TCT AAT CCT AGT TTG-3'). The thermal cycle profile after an initial 3-min denaturation at 95 °C was as follows (35 cycles): denaturation at 98 °C for 20 sec; annealing at 65 °C for 15 sec; and extension at 72 °C for 15 sec, with a final extension at the same temperature for 5 min. Eight replications were performed for the 1<sup>st</sup> PCR, and products were pooled in a single 1.5-ml tube. The pooled products were purified and size-selected for 200–400 bp using a SPRIselect (Beckman Coulter, Fullerton, CA, USA) to remove dimers and monomers following the manufacturer's protocol.

The second-round PCR (2<sup>nd</sup> PCR) was carried out with a 24-µl reaction volume containing 12 µl of 2× KAPA HiFi HotStart ReadyMix, 2.8 µl of each primer (5 µM), 4.4 µl of sterilized distilled H<sub>2</sub>O, and 2.0 µl of template. We used the

following two primers to append the dual-index sequences (eight nucleotides indicated by Xs) and flowcell-binding sites for the MiSeq platform (5' ends of the sequences before the eight Xs): 2<sup>nd</sup>-PCR-forward (5'-AAT GAT ACG GCG ACC ACC GAG ATC TAC ACX XXX XXX XAC ACT CTT TCC CTA CAC GAC GCT CTT CCG ATC T-3') and 2<sup>nd</sup>-PCR-reverse (5'-CAA GCA GAA GAC GGC ATA CGA GAT XXX XXX XXG TGA CTG GAG TTC AGA CGT GTG CTC TTC CGA TCT-3'). The thermal cycle profile after an initial 3-min denaturation at 95 °C was as follows (12 cycles): denaturation at 98 °C for 20 s; combined annealing and extension at 72 °C for 15 s, with a final extension at 72 °C for 5 min. The concentration of each 2<sup>nd</sup>-PCR product was measured by quantitative PCR using TB Green Fast qPCR Mix (TaKaRa, Otsu, Japan). Each sample was diluted to a fixed concentration and combined (i.e. one pooled 2<sup>nd</sup>-PCR product that included all samples). The pooled 2<sup>nd</sup>-PCR product was size-selected to approximately 370 bp using BluePippin (Sage Science, Beverly, MA, USA). The size-selected library was purified using Agencourt AMPure XP beads, adjusted to 4 nM by quantitative PCR using TB Green Fast qPCR Mix (TaKaRa, Otsu, Japan), and sequenced on the MiSeq platform using a MiSeq v2 Reagent Kit (Illumina, San Diego, CA, USA).

## Data preprocessing and taxonomic assignment

The raw MiSeq data were converted into FASTQ files using the bcl2fastq program provided by Illumina (bcl2fastq v2.18). The FASTQ files were then demultiplexed and the processed reads were subjected to a BLASTN search against the full NCBI database using Claident (Tanabe and Toju 2013). Reads where the sequence similarity between queries and the top BLASTN hit was < 98.5% and the sequence length was less than ≤ 150 bp were not used for the subsequent analyses. After BLASTN searches, the assembled sequences assigned to the same species were clustered, and the clustered sequences were treated as operational taxonomic units (OTUs). The OTUs whose sequence reads were < 0.05% of the total reads were considered a noise for each sample and thus excluded to remove possible contaminants. In the present study, after OTUs read by the above-mentioned methods were removed, the remaining OTUs were defined as a high-quality read. The numbers of DNA copies of each sample were estimated using methods described by Ushio et al. (2018) and Ushio (2019): first, the linear regression of five internal standard DNA copies and read numbers were used to estimate the standard curve, and then the curve was used to convert the read of each OTU to DNA copy numbers. At least three out of five internal standard DNA copies were detected samples that were used for subsequent analyses in the present study.

## Index of current direction relative to the AR (Dir)

The sea current field, i.e. the east-west velocity ( $u$ , eastward positive) and the north-south velocity ( $v$ , northward positive), was measured at multiple layers using a



ship-mounted 300-kHz ADCP (Teledyne RD Instruments, Poway, CA, USA). In subsequent analyses, velocity data from the layer at 47 m depth (excluding St. S3 where the depth was 23 m) were used. Both layers were close to the middle layer sampling depth zone. Velocity data were time-averaged for 7 min, i.e. from 3 min before the 1-min sampling time to 3 min after the sampling time (Suppl. material 1: Table S1). The parameter *Dir* (index of current direction relative to the AR) was introduced to evaluate the effect of the sea current direction relative to the AR on the distribution of eDNA density. The index *Dir* quantifies to what extent the current at each sampling station is directed toward the AR.

As illustrated in Fig. 2, the index *Dir* was defined as

$$Dir \equiv \vec{r} \cdot \vec{U} / U \quad (1)$$

where  $\vec{r}$  is the unit vector indicating the direction from the AR to each sampling station,  $\vec{U} = (u, v) = (U \cos \theta, U \sin \theta)$  is the velocity vector,  $U = (u^2 + v^2)^{0.5}$  is the absolute value of velocity,  $\theta$  is the current direction estimated from the time-averaged  $u$  and  $v$  data (0 degrees for the eastward direction and counter-clockwise positive), and the operator “ $\cdot$ ” denotes the inner product. By incorporating  $\vec{r} = (0, 1)$  for the northern stations,  $(0, -1)$  for the southern stations,  $(1, 0)$  for the eastern stations, and  $(-1, 0)$  for the western stations into equation (1), respectively, index *Dir* is expressed more specifically as  $\sin(\theta)$  (northern stations),  $-\sin(\theta)$  (southern),  $\cos(\theta)$  (eastern), and  $-\cos(\theta)$  (western). The value of *Dir* ranges from -1.0 to 1.0, where negative values (blue in Fig. 2) indicate upstream currents relative to the AR and positive values (red in Fig. 2) indicate downstream currents.

### Data analysis

As described in Results, the top four species with the largest amount of eDNA distribution were Japanese anchovy (*Engraulis japonicus*), threeline grunt (*Parapristipoma trilineatum*), chub mackerel (*Scomber* spp), and horse mackerel (*T. japonicus*) (Table 1). To examine the relationship between the eDNA density distribution of the four dominant species, and their distance from the AR and the current fields around the AR, general linear modeling (GLM) was used to create current-distribution models. These models, which assumed a normal distribution with an identity link function with a log-based eDNA density ( $\log(eDNA+0.1)$ ) as the response variable, and day (*Day*), distance from the AR (*Dist*), index of the relative current direction to the AR (*Dir*), velocity (*Vel*), and interaction between *Dir* and *Vel* (*Dir: Vel*) as explanatory variables, were created for the initial models. Akaike’s information criterion (AIC) and Bayesian information criterion (BIC) were then used to select the best model among the initial models. The Wald test was used to determine the significance for coefficients of the explanatory variables of the best models. The likelihood ratio test was used to compare the the best and null models. All statistical analyses were performed using R (version 4.0.4; R Development Core Team 2020).

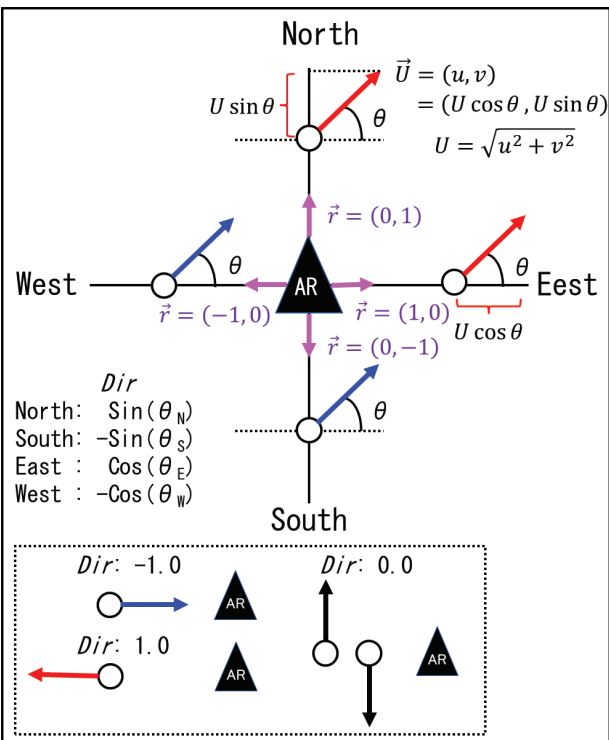


**Figure 2.** Schematic diagram for the calculation of the index *Dir*. *Dir* is defined as the inner product of the unit vector indicating the direction from the AR to each sampling station ( $\vec{r}$ ) and the velocity vector ( $\vec{U}$ ). By assuming  $\vec{r} = (0, 1)$  for the northern stations,  $(0, -1)$  for the southern stations,  $(1, 0)$  for the eastern stations, and  $(-1, 0)$  for the western stations, *Dir* is expressed more specifically as  $\sin(\theta)$  (northern),  $-\sin(\theta)$  (southern),  $\cos(\theta)$  (eastern), and  $-\cos(\theta)$  (western). The value of *Dir* ranges from -1.0 to 1.0, where the negative (blue color) and positive (red color) values respectively indicate upstream and downstream directions from the AR.

**Table 1.** Accession numbers and the number of eDNA copies for the 10 dominant species.

Acc. No.	Species	Rank			eDNA copies (copies L-1)	Sp copies / Total copies (%)
		Total	Day 1	Day 2		
LC468861.1	<i>Engraulis japonicus</i>	1	1	1	21,408.3	74.2
LC421693.1	<i>Parapristipoma trilineatum</i>	2	2	2	1,633.0	5.7
LC385179.1	<i>Scomber japonicus</i> or <i>S. australasicus</i>	3	3	4	748.8	2.6
LC385180.1	<i>Trachurus japonicus</i>	4	5	3	637.1	2.2
LC506661.1	<i>Spratelloides gracilis</i>	5	4	5	615.9	2.1
LC021031.1	<i>Maurollicus japonicus</i>	6	6	6	478.9	1.7
LC492390.1	<i>Seriola quinqueradiata</i>	7	8	9	370.0	1.3
LC421694.1	<i>Pagrus major</i>	8	9	8	365.2	1.3
LC385054.1	<i>Sardinops melanostictus</i>	9	12	7	353.5	1.2
LC385202.1	<i>Etrumeus teres</i>	10	7	10	340.3	1.2

## Results

### Sequence reads and quantification of eDNA copy numbers

The MiSeq paired-end sequencing of the 58 libraries, which comprised 54 field samples (Day 1: 30 samples, Day 2: 24 samples) and both a negative field sample and a PCR-level control sample on each day for this study, yielded a total of 7,054,162 reads with 94.0% base calls containing Phred quality scores of over 30.0 (Q30; error rate = 0.1%, or base call accuracy = 99.9%), and 6,877,676 (97.5%) were high-quality reads of which 3,735,725 (54.3%) were non-standard fish sequences, and 135 operational taxonomic units (OTUs), which included at least 117 genera, were detected (Suppl. material 1: Table S3). Excluding the standard DNA read numbers, the sequence reads of the two negative field controls were 0 and 1143 (0% and 7.1% of the mean DNA copy numbers of field-positive samples), and the sequence reads of the two PCR-level negative controls were 0 and 391 (0% and 0.57% of the mean DNA copy numbers of field-positive samples). This result indicated that serious contamination during field sampling and/or laboratory experiments did not occur or was insignificant. Data sets of three samples – one of which was collected from St. W2, one from the water surface at the AR, and one from its middle layer – were excluded from subsequent analyses, because three out of five standard DNAs were not detected in these samples (i.e. the sequence reads of these samples could not be converted to accurate eDNA densities). The sample-specific relationship between the sequence reads and the copy numbers of standard DNAs were examined using a linear regression. The mean  $r^2$  value of the regression lines was 0.96, and more than 84% of the samples had values greater than 0.9 (Fig. 3). This indicates that the read numbers of each OTU in each sample could be converted to a DNA copy number with minimal error using the method described by Ushio et al (2018).

The top ten species with the eDNA distribution are shown in Table 1. The present study focused on four dominant species that accounted for a total of 84.7% of the total number of DNA copies: 74.2% was for Japanese anchovy (*E. japonicus*); 5.7% for threeline grunt (*P. trilineatum*); 2.6% for chub mackerel (*Scomber* spp), which could not be identified as either *S. japonicus* or *S. australasicus* from the nucleotide sequence; and 2.2% for horse mackerel (*T. japonicus*) (Table 1).

### Current fields around the AR

Based on the ADCP data, current velocity and the direction at each sampling station are shown in Fig. 4. Current velocity on Day 1 was larger than that on Day 2, and north-west and northeast currents were prevalent, while on Day 2, west and southwest currents were prevalent. On Day 1, the indices of current direction relative to the AR ( $Dir$ ) were negative ( $Dir < 0$ ) at the three southern stations (S1, S2 and S3), one eastern station (E3), and two western stations (W2 and W3). Waters to the south and west of the AR

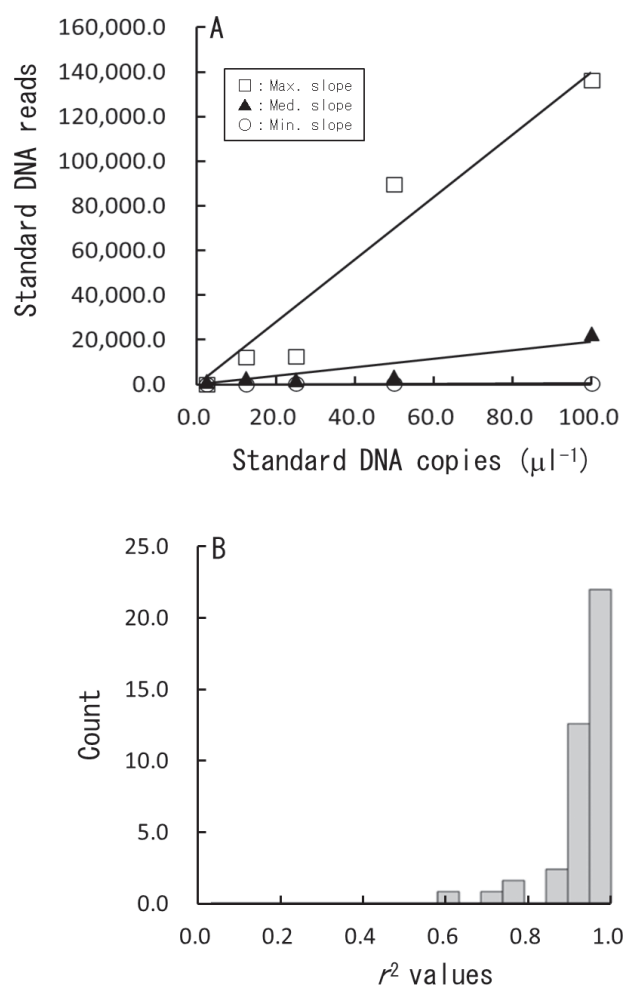


**Figure 3.** Relationships between sequence reads and copy numbers of standard DNAs according to Ushio et al. (2018). Relationships between sequence reads and copy numbers of standard DNAs with maximum (open squares), median (black triangles), and minimum (open circles) slopes (A). Distribution of  $r^2$  values of the regression lines (B).

were thus upstream of the current on Day 1. On Day 2,  $Dir$  was negative ( $Dir < 0$ ) at one northern station (N2) and the three eastern stations (E1, E2 and E3). Waters to the east of the AR were thus upstream of the current on Day 2.

### Spatial distribution of fish eDNA densities around the AR

Spatial distributions of the eDNA densities for the four species are shown in Suppl. material 2: Figs S1–S4. In the case of *E. japonicus* (Suppl. material 2: Fig. S1), eDNA density at the AR was 5 to 30 times higher than at the other stations except for two western stations (W2 and W3), which were upstream of the AR on Day 1 (Fig. 4). On Day 2, eDNA density was low overall, just 1/30 of the mean density on Day 1 at the AR. However, the eastern stations, which were upstream of the AR, had the highest eDNA densities. In the case of *P. trilineatum* (Suppl. material 2: Fig. S2), eDNA density on Day 1 was the highest at western St. W2, which was upstream of the AR compared to the other stations. On Day 2, eDNA densities for *P. trilineatum*

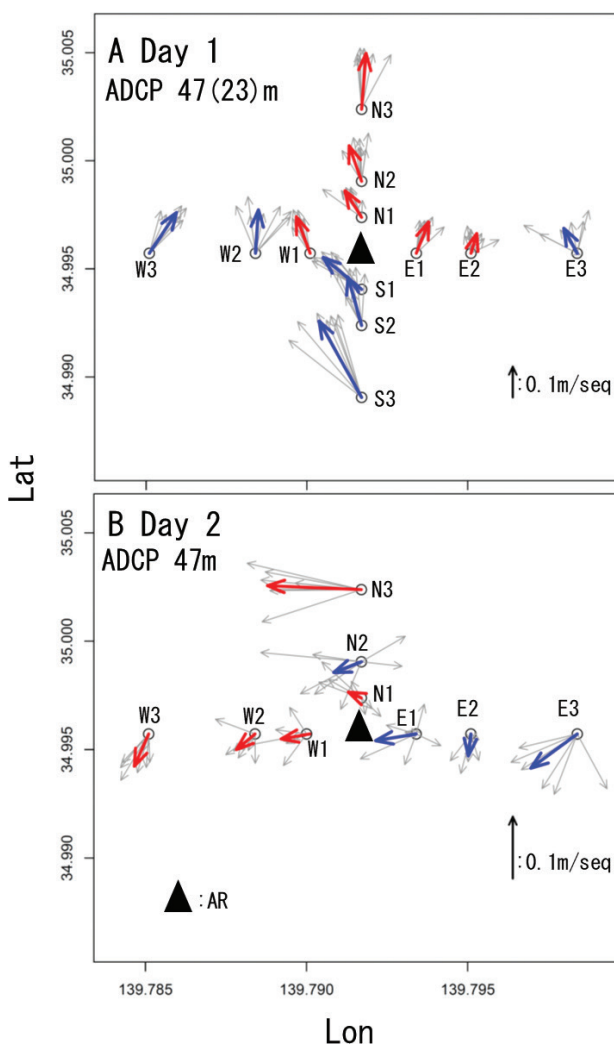


**Figure 4.** Current direction and velocity at each station on Day 1 (A) and Day 2 (B). Blue and red arrows indicate the mean of 7-min ADCP data and show the upstream ( $Dir < 0$ ) and downstream ( $Dir > 0$ ) currents, respectively. Gray arrows show the current and velocity mean of each minute.

as well as the other species at two eastern stations (E1 and E3) were higher than at the other stations. In the case of *Scomber* spp (*S. japonicus* or *S. australasicus*) (Suppl. material 2: Fig. S3) as well as *E. japonicus* and *P. trilineatum*, on Day 1, eDNA densities at two western stations (W2 and W3) were higher than at the other stations. On Day 2, eDNA densities for all four species at two eastern stations (E1 and E3) were higher than at the other stations except for *Scomber* spp at St. W1. In the case of *T. japonicus* (Suppl. material 2: Fig. S4), eDNA density on Day 1 at St. S1, which was upstream of the AR, was higher than it was at the other stations, and eDNA densities at the southern stations decreased with increasing distance from the AR.

#### Effects of distance and current direction from the AR on fish eDNA densities

To examine the relationship between eDNA density and current fields for the four species, we created current-distribution models based on the GLMs. The results of mod-

el selection and statistical parameters of best models are shown in Tables 2, 3, respectively.

In the case of *E. japonicus*, out of five explanatory variables in the first model (AIC=147.567; BIC=159.565), *Day*, *Dist* and *Dir* were selected as explanatory variables in the best models (AIC=145.076; BIC=153.644) by AIC selection. Furthermore, *Dist* was removed from the best models by BIC selection, and *Day* and *Dir* were selected as explanatory variables in the BIC-based best models (AIC=146.184; BIC=153.038). Best models selected by AIC and BIC were significantly different from the null models (likelihood ratio test, AIC model: DF (37, 40),  $-2\log L = -32.632$ ,  $p < 0.001$ ; BIC model: DF (38, 40),  $-2\log L = -27.535$ ,  $p < 0.001$ ). For the AIC-based best model, coefficients of two explanatory variables (*Day* and *Dir*) were significant (Wald test, *Day*:  $t = -3.120$ ,  $p = 0.004$ ; *Dir*:  $t = -2.697$ ,  $p = 0.012$ , respectively) and *Dist* was not significant ( $t = -1.707$ ,  $p = 0.096$ ). However, the deviance explained (%) of the AIC-selected model was 33.5%, which was higher than that of the BIC-selected model (28.3%), while the difference between the BIC in both models (delta BIC) was as small as 0.61, indicating an insignificant difference between both best models (likelihood ratio test, df (38,37),  $-2\log L = 5.097$ ,  $p > 0.05$ ). The AIC-based best model was thus used to predict eDNA density, as described below.

For both *P. trilineatum* and *Scomber* spp, out of five explanatory variables in the first models (*P. trilineatum*: AIC=179.985, BIC=191.980; *Scomber* spp: AIC=205.562, BIC=217.557), *Dir* was selected as an explanatory variable in the best models (*P. trilineatum*: AIC=173.644, BIC=178.785; *Scomber* spp: AIC=199.822, BIC=204.962) by both model selections.

In the case of *T. japonicus*, out of five explanatory variables in the first model (AIC=185.173; BIC=197.168), *Dist* and *Dir* were selected as explanatory variables in the best models (AIC=182.465; BIC=189.319) by AIC selection. Furthermore, *Dist* was removed from the best models by BIC selection, and *Dir* was selected as an explanatory variable in the BIC-based best models (AIC=183.528; BIC=188.669). The best models selected by AIC and BIC were significantly different from the null models (likelihood ratio test, AIC model: DF (38, 40),  $-2\log L = -37.409$ ,  $p < 0.05$ ; BIC model: DF (39, 40),  $-2\log L = -24.286$ ,  $p < 0.05$ ). For the AIC-based best model, the coefficient of *Dir* was significant (Wald test,  $t = -2.626$ ,  $p = 0.012$ ) and that of *Dist* was not significant (Wald test,  $t = -1.717$ ,  $p = 0.094$ ). However, the deviance explained (%) of the AIC-selected model in the case of *T. japonicus* was 18.1%, which was also higher than that of the BIC-selected model (11.1%), and the difference between BIC in both models (delta BIC), at 0.65, was almost equally small, again indicating an insignificant difference between both best models (likelihood ratio test, df (39,38),  $-2\log L = 13.123$ ,  $p > 0.05$ ). As with *E. japonicus*, the AIC-based best model was used to predict eDNA density for *T. japonicus*, too.

Using the best models, eDNA density in relation to *Dir* was predicted for the four species as follows (Figs 5–8): in the case of *E. japonicus* (Fig. 5), we

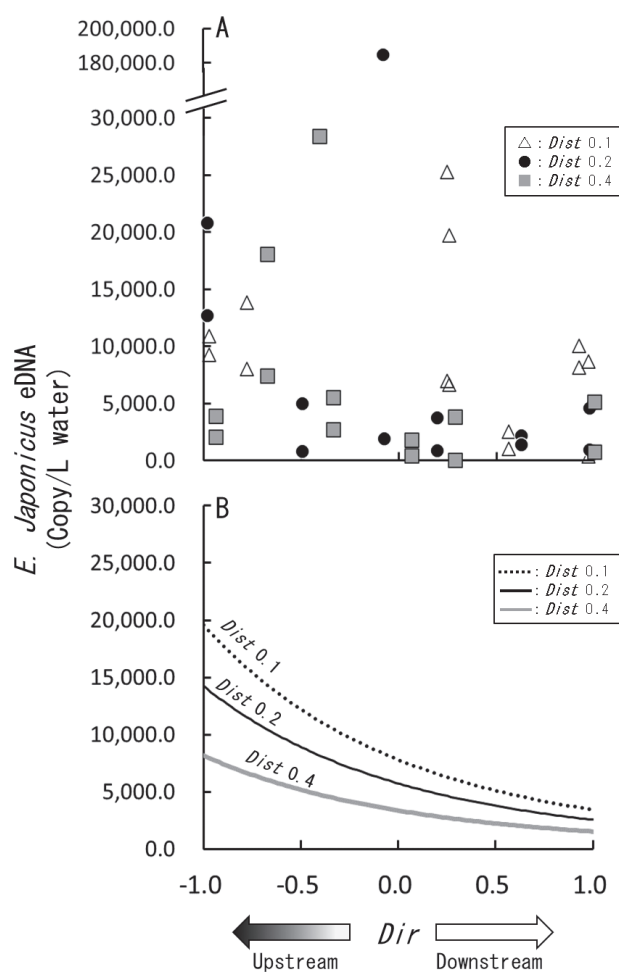


**Figure 5.** Relationship between the index of relative current direction to the AR (*Dir*) and eDNA copies (A) and predicted eDNA copies (B) of *Engraulis japonicus*. *Dir* values range from -1.0 to 1.0. Negative values (*Dir* < 0) indicate upstream currents and positive values (*Dir* > 0) indicate downstream currents. Open triangles, black circles, and gray squares of (A) show the number of eDNA copies at *Dist* 0.1, 0.2, and 0.4, respectively. The dotted, solid, and gray lines of (B) show the predicted number of eDNA copies at *Dist* 0.1, 0.2, and 0.4, respectively.

predicted the eDNA density for LSmean of *Day* when *Dir* varied from -1 to 1 at *Dist* 0.1, 0.2, and 0.4 miles; for *P. trilineatum* (Fig. 6) and *Scomber* spp (Fig. 7), we predicted the eDNA density when *Dir* varied from -1 to 1; and in the case of *T. japonicus*, we predicted the eDNA density when *Dir* varied from -1 to 1 at *Dist* 0.1, 0.2, and 0.4 miles (Fig. 8). A similar trend was observed for all species in the relationship between eDNA density and *Dir*, i.e. the eDNA density of all species reached the maximum *Dir* at -1.0, which refers to the upstream side, and eDNA density rapidly decreased with an increase of *Dir*. In addition to *Dir*, *Day* and *Dist* were selected for the AIC-based best model in the case of *E. japonicus*, and *Dist* was selected for the AIC-based best model in the case of *T. japonicus* (Table 2). The pattern of eDNA density distribution was similar for both species: the more upstream and the closer to the AR the distribution was, the denser the eDNA was predicted to be (Figs 5, 8).

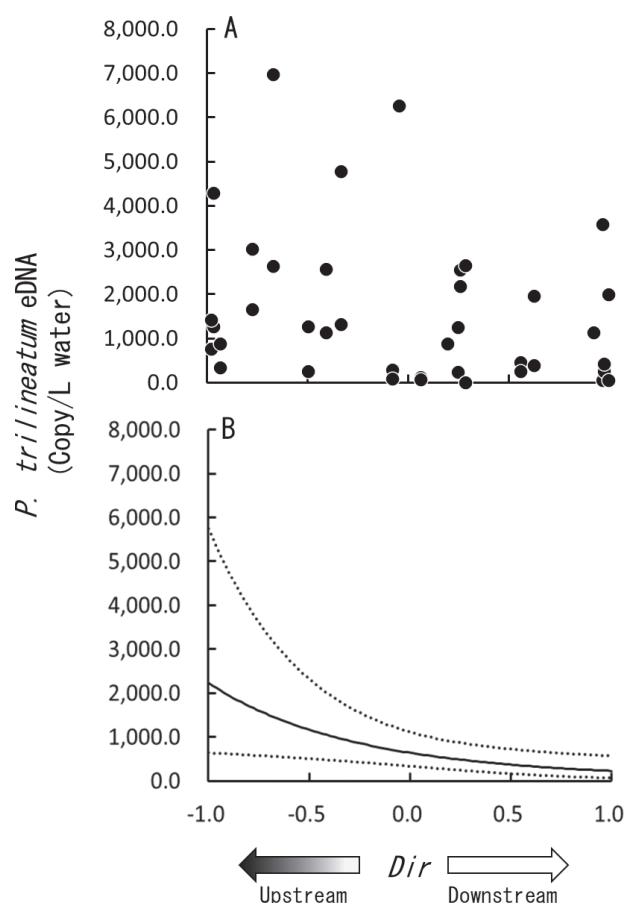


**Figure 6.** Relationship between the index of relative current direction to the AR (*Dir*) and number of eDNA copies (A) and predicted number of eDNA copies (B) of *Parapristipoma trilineatum*. The solid line and dotted lines of (B) show the predicted number of eDNA copies and 95% confidence intervals, respectively.

## Discussion

The number of studies utilizing eDNA to examine the spatio-temporal distribution of marine vertebrates has been increasing in recent years (Lacoursière-Roussel et al. 2016; Yamamoto et al. 2016; Stoeckle et al. 2017; Sato et al. 2021). Previous studies have found a positive relationship between the abundance of target species and eDNA density in semi-enclosed marine systems (Yamamoto et al. 2016; Stoeckle et al. 2017), and our previous research conducted in the same waters of the present study found similar associations in an open marine system (Sato et al. 2021). Additionally, recent studies on natural fish abundances also showed that eDNA density in water samples provided similar fish abundance indices such as catch per unit effort (CPUE) used in fisheries management (Lacoursière-Roussel et al. 2016). Fukaya et al. (2020) successfully estimated the population abundance of *T. japonicus* in semi-enclosed Maizuru Bay by combining eDNA data from quantitative PCR, experimental results of the production and degradation process of eDNAs, and hydrodynamic modeling.

As an average effect of ARs within periods ranging from a few months to years, the highest density of fish schools is typically formed directly above the AR, and the density



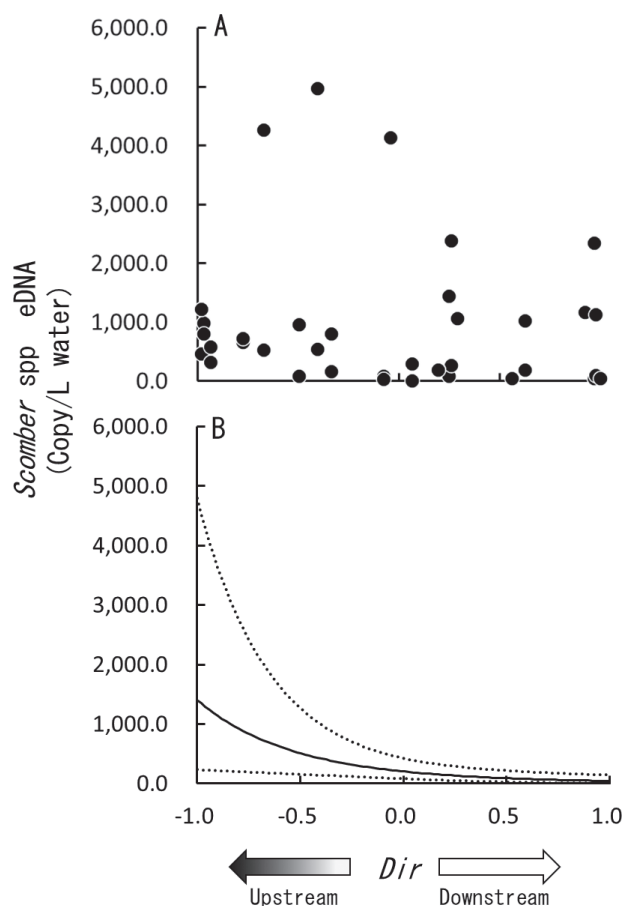


**Figure 7.** Relationship between the index of relative current direction to the AR (*Dir*) and number of eDNA copies (A) and number of predicted eDNA copies (B) of *Scomber* spp. (*S. japonicus* or *S. australasicus*). The solid line and dotted lines of (B) show the predicted number of eDNA copies and 95% confidence intervals, respectively.

decreases with increasing distance from the AR (Boswell et al. 2010; Scott et al. 2015; Inoue et al. 2018, 2020). In more detailed fish school formations at the diurnal variation level, dense fish schools are formed in the upstream side of ARs (Kakimoto 1967; Okamoto et al. 1979; Lindquist and Pietrafesa 1989; Holland et al. 2021). If we assume that the origin of eDNA is formed directly above or at the upstream side of an AR and eDNA density is simply affected by distance and current, a high density of eDNA would distribute downstream from the AR, and eDNA density would probably decrease with distance from the AR and with increasing current velocity in surrounding waters.

The present study focused on four species (*E. japonicus*, *P. trilineatum*, *Scomber* spp, and *T. japonicus*) whose eDNA was dominant and target species except *E. japonicus* were commonly caught in set-net fisheries at Tateyama Bay (Suppl. material 1: Table S4). *E. japonicus* was not in the list of the set-net fisheries because this species was not targeted by this fishery. In the case of all species, *Dir* was selected as the explanatory variable of best models by both AIC- and BIC-based selection. In addition, the eDNA densities of all species, which were predicted by the models, were greatest at a *Dir* of -1.0, which points to the upstream side, and eDNA density

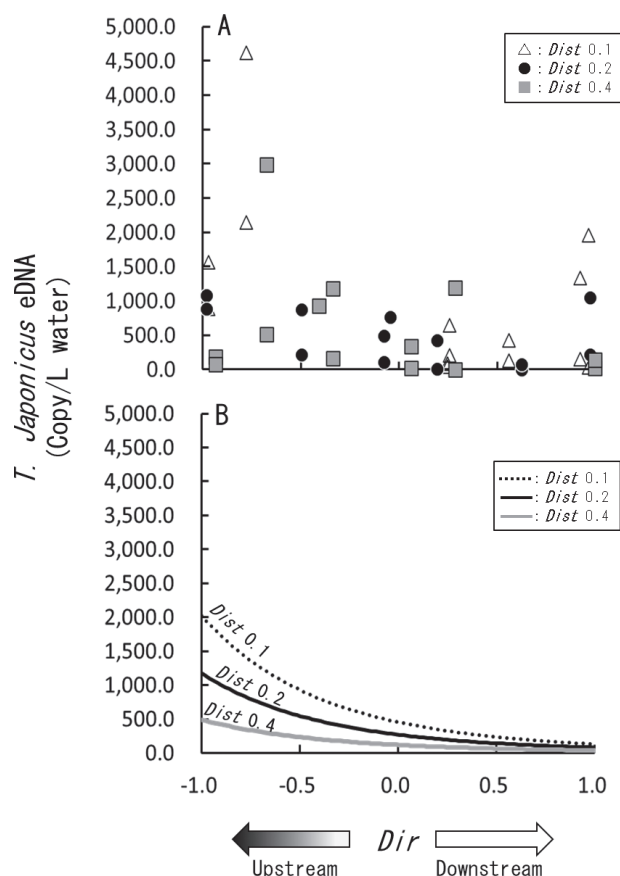


**Figure 8.** Relationship between the index of relative current direction to the AR (*Dir*) and number of eDNA copies (A) and predicted number of eDNA copies (B) of *Trachurus japonicus*. Open triangles, black circles, and gray squares of (A) show the number of eDNA copies at *Dist* 0.1, 0.2, and 0.4, respectively. The dotted, solid, and gray lines of (B) show the predicted number of eDNA copies at *Dist* 0.1, 0.2, and 0.4, respectively.

rapidly decreased with the increase of *Dir* (Figs 5–8) without effect from current velocity. The tendencies of eDNA density distribution in this study are in accord with the tendency of actual fish distribution described above. Judging from the results of eDNA density distribution patterns related to *Dir*, the present study demonstrates that eDNA density distribution is more influenced by actual distribution patterns of fish than by a transport process affected by currents.

Our previous study reported on a similar phenomenon in the relationship between distance and eDNA density distribution for several fish species: the eDNA density of *P. trilineatum*, *P. major*, and *T. japonicus* in particular clearly decreased even 150 m from the AR (Sato et al. 2021). A similar trend was observed for *E. japonicus* on Day 1, where eDNA density at the AR was 5 to 30 times higher than at the other stations except for two western stations (W2 and W3) that were upstream (Suppl. material 2: Fig. S1). In the case of other fish species, eDNA density tended to distribute at average levels or higher at the AR than at other stations except for the upstream stations, however no high distribution was observed at the AR (Suppl. material 2: Figs S1–S4).

**Table 2.** Statistical parameters and explanatory variables of the current-distribution models.

Species	Model	Explanatory variable						Deviance explained (%)	Information criterion		$r^2$
		Day	Dist	Dir	Vel	Day:Dist			BIC	AIC	
<i>Engraulis japonicus</i>	First model	+	+	+	+	+		35.9	159.565	147.567	0.268
	Best model							28.3	153.038	146.184	0.245
	AIC-based	+	+	+				33.5	153.644	145.076	0.281
<i>Parapristipoma trilineatum</i>	First model	+	+	+	+	+		17.5	191.980	179.985	0.058
	Best model							14.1	178.785	173.644	0.119
	AIC-based							14.1	178.785	173.644	0.119
<i>Scomber japonicus</i> or <i>S. australasicus</i>	First model	+	+	+	+	+		21.1	217.557	205.562	0.099
	Best model							16.7	204.962	199.822	0.145
	AIC-based							16.7	204.962	199.822	0.145
<i>Trachurus japonicus</i>	First model	+	+	+	+	+		24.4	197.168	185.173	0.136
	Best model							11.8	188.669	183.528	0.095
	AIC-based		+	+				18.1	189.319	182.465	0.138

Of the four species, *Dist* was selected as the explanatory variable in the best model selected by AIC for *E. japonicus* and *T. japonicus*, however the result of the Wald test was not significant and *Dist* was omitted from the best model selected by BIC (Tables 2, 3). In the cases of both *E. japonicus* and *T. japonicus*, the differences between the BIC-based models with and without *Dist* (delta BIC) were small and not significant (likelihood ratio test,  $p > 0.05$ ). In this study, models including *Dist* were therefore adopted to predict the distribution of eDNA density for these two species. The pattern of eDNA density distribution was similar for both species: the more upstream and the closer to the AR the distribution was, the denser the eDNA was predicted to be (Figs 5, 8).

In the present study, AR proximity station data were omitted from the modeling because we mainly focused on the relationship between eDNA density distribution and *Dir*. Therefore, the effect of *Dist* may have been underestimated for some target species. For example, both AIC and BIC excluded *Dist* from the explanatory variables for *P. trilineatum* while there was a strong relationship between eDNA density and distance from the AR in Sato et al. (2021). In addition, there is a possibility that prey abundance or other environmental factors temporarily varied between the two study periods, and such circumstances may change the relationship between the eDNA density and distance from the AR for these species. The further accumulation of data and improvement of analysis methods are tasks to be undertaken in the future. Density distribution of the eDNA should be discussed by comparing the behavior of each species, such as migration and localization to the AR. This is a topic that was not possible in the present study. Among the four species, Ito (2011) studied the behavior of *T. japonicus* around ARs and found that this species stayed near the AR during the day, and at night migrated in a radius of about 3 km around the AR. Other than Ito (2011), however, very few studies have quantitatively clarified fish behavior around ARs installed in deep waters. According to Holland et al. (2021), the probability of school occurrence declined with increasing distance from the AR, although the preference for upstream orientation among schools was almost twice as great as it was downstream. As Holland et al. (2021) pointed out, in the cases of *E. japonicus* and *T. japonicus*, distance from the AR and current direction relative to the AR were

**Table 3.** Statistical parameters and explanatory variables of the best models.

Species	Explanatory variable	Estimate	Standard error	t value	p value <sup>1</sup>
<i>Engraulis japonicus</i>	Intercept	9.634	0.480	20.072	<0.001
	Day	-1.299	0.416	-3.120	0.004
	Dist	-2.851	0.416	-1.707	0.096
	Dir	-0.855	1.670	-2.697	0.010
<i>Parapristipoma trilineatum</i>	Intercept	6.419	0.299	6.419	<0.001
	Dir	-1.141	0.450	12.125	0.015
<i>Scomber japonicus</i> or <i>S. australasicus</i>	Intercept	5.235	0.412	5.235	<0.001
	Dir	-1.731	0.620	-1.731	0.008
<i>Trachurus japonicus</i>	Intercept	6.458	0.707	6.458	<0.001
	Dist	-4.574	2.664	-4.574	0.094
	Dir	-1.328	0.506	-1.328	0.012

1: p values of the Wald test.

interrelated, at least for eDNA density distribution, which indicated the spatio-temporal distribution of the fish.

In this study we examined the relationship between fish eDNA density and current fields, but a future study needs to compare eDNA density distribution patterns and fish abundance estimated by other methods (e.g., surveys using fishing gear, echo sounder surveys, and underwater drone, a technology that has developed rapidly in recent years) to confirm an actual link between fish and eDNA distributions in the field. In addition, other environmental factors such as water temperature and salinity, and also species composition, which includes the presence of predators and prey, also have an influence on fish and eDNA distributions. Examining such factors in future studies may uncover more detailed fish behavior and prey-predator interactions around ARs.

## Conclusions

A new AR monitoring method is required to compensate for disadvantages of traditional methods such as visual censuses, surveys using fishing gear, and echo sounder. eDNA distribution reflects not only the spatio-temporal distribution of fish but also degradation and transport. An understanding of the relationship between current fields and eDNA distribu-

tion, particularly in open waters, is critical when using eDNA as an index for fish aggregation at ARs. We investigated the relationship between eDNA distribution and current fields around an AR for four dominant species in Tateyama Bay, Japan. The present study demonstrates that eDNA density distribution is more influenced by actual distribution patterns of fish than by a transport process affected by currents.

## Data availability

DDBJ accession numbers of the DNA sequences analyzed in the present study are PSUB016911 (Submission ID), PRJDB13123 (BioProject ID) and SAMD00445249–SAMD00445303 (BioSample ID).

## Conflicts of interest

The authors declare that they have no conflicts of interest.

## Contributions

N.I., M.S., N.F. and T.I. designed the study and conducted field surveys. N.I. and M.S. performed molecular experiments, and M.U. prepared the internal standards for eDNA quantification. N.I. and M.S. analyzed the fish community dataset extracted from results of MiSeq sequencing. N.I. and N.F. analyzed the ADCP dataset. N.I. wrote the first draft of the manuscript and other authors made significant contributions with comments on the manuscript.

## Acknowledgements

We are grateful to the staff of the research vessel Takamaru for their support in the field, Tomoe Ishibashi of Fisheries Technology Institute, and Tomoyasu Shirako of IDEA Consultants, Inc. for support in molecular experiments. We are grateful to Hasama Fisheries Cooperative for providing their fish catch data of the set net. This work was supported by the research grants from the National Research Institute of Fisheries Engineering (NRIFE) in fiscal year 2018–2019.

## References

- Barnes MA, Turner CR (2016) The ecology of environmental DNA and implications for conservation genetics. *Conservation Genetics* 17(1): 1–17. <https://doi.org/10.1007/s10592-015-0775-4>
- Bohnsack JA, Sutherland DL (1985) Artificial reef research: A review with recommendations for future priorities. *Bulletin of Marine Science* 37: 11–39.
- Boswell KM, Wells RJ, Cowan Jr JH, Wilson CA (2010) Biomass, density, and size distributions of fishes associated with a largescale artificial reef complex in the Gulf of Mexico. *Bulletin of Marine Science* 86(4): 879–889. <https://doi.org/10.5343/bms.2010.1026>
- Fukaya K, Murakami H, Yoon S, Minami K, Osada Y, Yamamoto S, Masuda R, Kasai A, Miyashita K, Minamoto T, Kondoh M (2020) Estimating fish population abundance by integrating quantitative data on environmental DNA and hydrodynamic modelling. *Molecular Ecology* 30(13): 3057–3067. <https://doi.org/10.1111/mec.15530>
- Goldberg CS, Turner CR, Deiner K, Klymus KE, Thomsen PF, Murphy MA, Murphy MA, Spear SF, McKee A, Oyler-McCance SJ, Cornman RS, Laramie MB, Mahon AR, Lance RF, Pilliod DS, Strickler KM, Waits LP, Fremier AK, Takahara T, Herder JE, Taberlet P (2016) Critical considerations for the application of environmental DNA methods to detect aquatic species. *Methods in Ecology and Evolution* 7(11): 1299–1307. <https://doi.org/10.1111/2041-210X.12595>
- Holland MM, Becker A, Smith JA, Everett JD, Suthers IM (2021) Fine-scale spatial and diel dynamics of zooplanktivorous fish on temperate rocky and artificial reefs. *Marine Ecology Progress Series* 674: 221–239. <https://doi.org/10.3354/meps13831>
- Inoue N, Nanbu R, Kuwahara H, Kumamoto J, Yokoyama J, Kanaiwa M (2018) The present situation of utilization and the effects of artificial reefs on the resource density of Japanese butterfish *Hyperoglyphe japonica* and red sea bream *Pagrus major* in the waters of the Iki Islands, Nagasaki, Japan. *Nippon Suisan Gakkaishi* 84: 1010–1016. <https://doi.org/10.2331/suisan.17-00081> [In Japanese with English abstract]
- Inoue N, Kuwahara H, Manbu R, Ishimaru S, Hashimoto K, Kuwamoto J, Masubuchi T, Kanaiwa M (2020) Estimation of artificial reef effect range in the waters of Tsushima Islands, Nagasaki, Japan. *Bulletin of the Japanese Society of Fisheries Oceanography* 84: 187–199. [Japanese with English abstract]
- Itô Y (2011) Artificial Reef Function in Fishing Grounds off Japan. In: Bortone SA, Pereira BF, Fabi G, Otake S (Eds) *Artificial reefs in fisheries management*. CRS press, New York, 239–264.
- Kakimoto H (1967) On the effective areas of the artificial reefs. *Suisan Zoshoku* 14: 181–198.
- Kakimoto H (1993) Control of fish behavior by the artificial reef. *Fisheries Engineering* 30: 59–68.
- Kang M, Nakamura T, Hamano A (2011) A methodology for acoustic and geospatial analysis of diverse artificial-reef datasets. *ICES Journal of Marine Science* 68(10): 2210–2221. <https://doi.org/10.1093/icesjms/fsr141>
- Komai T, Gotoh RO, Sado T, Miya M (2019) Development of a new set of PCR primers for eDNA metabarcoding decapod crustaceans. *Metabarcoding and Metagenomics* 3: 1–19. <https://doi.org/10.3897/mbmg.3.33835>
- Lacoursière-Roussel A, Côté G, Leclerc V, Bernatchez L (2016) Quantifying relative fish abundance with eDNA: A promising tool for fisheries management. *Journal of Applied Ecology* 53(4): 1148–1157. <https://doi.org/10.1111/1365-2664.12598>
- Lima SJ, Zalmon IR, Love M (2019) Overview and trends of ecological and socioeconomic research on artificial reefs. *Marine Environmental Research* 149: 81–96. <https://doi.org/10.1016/j.marenvres.2019.01.010>
- Lindquist DG, Pietrafesa LJ (1989) Current vortices and fish aggregations: The current field and associated fishes around a tugboat wreck in Onslow Bay, North Carolina. *Bulletin of Marine Science* 44: 533–544.
- Minamoto T, Fukuda M, Katsuhara KR, Fujiwara A, Hidaka S, Yamamoto S, Takahashi K, Masuda R (2017) Environmental DNA reflects spatial and temporal jellyfish distribution. *PLoS ONE* 12(2): e0173073. <https://doi.org/10.1371/journal.pone.0173073>
- Miya M, Sato Y, Fukunaga T, Sado T, Poulsen JY, Sato K, Minamoto T, Yamamoto S, Yamanaka H, Araki H, Kondoh M, Iwasaki W

- (2015) MiFish, a set of universal PCR primers for metabarcoding environmental DNA from fishes: Detection of more than subtropical marine species. *Royal Society Open Science* 2(7): 150088. <https://doi.org/10.1098/rsos.150088>
- Miya M, Minamoto T, Yamanaka H, Oka S, Sato K, Yamamoto S, Sado T, Doi H (2016) Use of a filter cartridge for filtration of water samples and extraction of environmental DNA. *Journal of Visualized Experiments* 25(117): 54741. <https://doi.org/10.3791/54741>
- Murakami H, Yoon S, Kasai A, Minamoto T, Yamamoto S, Sakata MK, Horiuchi T, Sawada H, Kondoh M, Yamashita Y, Masuda R (2019) Dispersion and degradation of environmental DNA from caged fish in a marine environment. *Fisheries Science* 85(2): 327–337. <https://doi.org/10.1007/s12562-018-1282-6>
- Okamoto O, Kuroki T, Murai T (1979) Fundermatal studies on the ecology of fishes near artificial reefs-I. *Nippon Suisan Gakkaishi* 45(9): 1085–1090. <https://doi.org/10.2331/suisan.45.1085> [Japanese with English abstract]
- Polovina JJ, Sakai I (1989) Impacts of artificial reefs on fishery production in Shimamaki, Japan. *Bulletin of Marine Science* 44: 997–1003.
- Port JA, O'Donnell JL, Romero-Maraccini OC, Leary PR, Litvin SY, Nickols KJ, Yamahara KM, Kelly RP (2016) Assessing vertebrate biodiversity in a kelp forest ecosystem using environmental DNA. *Molecular Ecology* 25(2): 527–541. <https://doi.org/10.1111/mec.13481>
- R Development Core Team (2020) R: A language and environment for statistical computing. R Foundation for Statistical Computing, Vienna, Austria.
- Sato M, Inoue N, Nambu R, Furuichi N, Imaizumi T, Ushio M (2021) Quantitative assessment of multiple fish species around artificial reefs combining environmental DNA metabarcoding and acoustic survey. *Scientific Reports* 11(1): 19477. <https://doi.org/10.1038/s41598-021-98926-5>
- Scott ME, Smith JA, Lowry MB, Taylor MD, Suthers IM (2015) The influence of an offshore artificial reef on the abundance of fish in the surrounding pelagic environment. *Marine and Freshwater Research* 66(5): 429–437. <https://doi.org/10.1071/MF14064>
- Stoeckle MY, Soboleva L, Charlop-Powers Z (2017) Aquatic environmental DNA detects seasonal fish abundance and habitat preference in an urban estuary. *PLoS ONE* 12(4): e0175186. <https://doi.org/10.1371/journal.pone.0175186>
- Taberlet P, Bonin A, Coissac E (2018) *Environmental DNA: For Biodiversity Research and Monitoring*. Oxford Academic, Oxford. <https://doi.org/10.1093/oso/9780198767220.001.0001>
- Tanabe AS, Toju H (2013) Two new computational methods for universal DNA barcoding: A benchmark using barcode sequences of bacteria, Archaea, animals, fungi, and land plants. *PLoS ONE* 8(10): e76910. <https://doi.org/10.1371/journal.pone.0076910>
- Ushio M (2019) Use of a filter cartridge combined with intra-cartridge bead-beating improves detection of microbial DNA from water samples. *Methods in Ecology and Evolution* 10(8): 1142–1156. <https://doi.org/10.1111/2041-210X.13204>
- Ushio M, Murakami H, Masuda R, Sado T, Miya M, Sakurai S, Yamanaka H, Minamoto T, Kondoh M (2018) Quantitative monitoring of multispecies fish environmental DNA using high-throughput sequencing. *Metabarcoding and Metagenomics* 2: 1–15. <https://doi.org/10.1101/113472>
- Yamamoto S, Minami K, Fukaya K, Takahashi K, Sawada H, Murakami H, Tsuji S, Hashizume H, Kubonaga S, Horiuchi T, Hongo M, Nishida J, Okugawa Y, Fujiwara A, Fukuda M, Hidaka S, Suzuki KW, Miya M, Araki H, Yamanaka H, Maruyama A, Miyashita K, Masuda R, Minamoto T, Kondoh M (2016) Environmental DNA as a 'snapshot' of fish distribution: A case study of Japanese jack mackerel in Maizuru Bay, Sea of Japan. *PLoS ONE* 11(3): e0149786. <https://doi.org/10.1371/journal.pone.0149786>
- Yamamoto S, Masuda R, Sato Y, Sado T, Araki H, Kondoh M, Minamoto T, Miya M (2017) Environmental DNA metabarcoding reveals local fish communities in a species-rich coastal sea. *Scientific Reports* 7(1): 40368. <https://doi.org/10.1038/srep40368>

## Supplementary material 1

### Tables S1–S4

Author: Nariaki Inoue, Masaaki Sato, Naoki Furuichi, Tomohito Imaizumi and Masayuki Ushio

Data type: Supplementary tables (Excel file)

Explanation note: **Table S1.** Details of the sampling stations for present study on June 3 (Day 1) and 4 (Day 2), 2019. **Table S2.** Sequences of the five standard DNAs conceived by Ushio et al. (2018) used in this study. **Table S3.** Accession numbers and the number of eDNA copies for all OTU species. **Table S4.** Species list of fish catch (kg) by a set net near study site in June 2019.

Copyright notice: This dataset is made available under the Open Database License (<http://opendatacommons.org/licenses/odbl/1.0/>). The Open Database License (ODbL) is a license agreement intended to allow users to freely share, modify, and use this Dataset while maintaining this same freedom for others, provided that the original source and author(s) are credited.

Link: <https://doi.org/10.3897/mbmg.6.87415.suppl1>

## Supplementary material 2

### Figures S1–S4

Author: Nariaki Inoue, Masaaki Sato, Naoki Furuichi, Tomohito Imaizumi and Masayuki Ushio

Data type: Supplementary figures (PDF file)

Explanation note: **Figure S1.** eDNA distribution pattern of *Engraulis japonicus* at the AR and three distances (Dist 0.1, 0.2, and 0.4 miles) from the AR in four directions. Bars with oblique lines show the number of eDNA copies at the AR, and black and white bars show the number of eDNA copies at upstream and downstream stations from the AR, respectively. **Figure S2.** eDNA distribution pattern of *Parapristipoma trilineatum* at the AR and three distances (Dist 0.1, 0.2, and 0.4 miles) from the AR in four directions. Symbols are the same as in Fig. S1. **Figure S3.** eDNA distribution pattern of *Scomber* spp. (*S. japonicus* or *S. australasicus*) at the AR and three distances (Dist 0.1, 0.2, and 0.4 miles) from the AR in four directions. Symbols are the same as in Figure S1. **Figure S4.** eDNA distribution pattern of *Trachurus japonicus* at the AR and three distances (Dist 0.1, 0.2, and 0.4 miles) from the AR in four directions. Symbols are the same as in Fig. S1.

Copyright notice: This dataset is made available under the Open Database License (<http://opendatacommons.org/licenses/odbl/1.0/>). The Open Database License (ODbL) is a license agreement intended to allow users to freely share, modify, and use this Dataset while maintaining this same freedom for others, provided that the original source and author(s) are credited.

Link: <https://doi.org/10.3897/mbmg.6.87415.suppl2>